ATTITUDE ACCURACY IMPROVEMENT OF ULTRA LOW-GRADE MEMS INS USING ALIGNMENT OF GPS ANTENNA

Masaru Naruoka
The University of Tokyo

Keywords: *INS/GPS Integration, MEMS, Sensor Fusion, Kalman Filtering, Low Cost Navigation*

Abstract

This paper proposes a method to improve the accuracy of attitude estimation of an ultra low-grade inertial navigation system (INS) by integration of a global position system (GPS) receiver and smart placement of the GPS antenna. This study is motivated by a previous work [2], which showed that integration by means of Kalman filtering of an inertial measurement unit (IMU) composed of low accuracy components, such as micro-electro-mechanical system (MEMS) gyros, and a GPS receiver, does not effectively have good accuracy of the attitude, especially the heading. This is mainly because of the low observability of the attitude, which can neither be correctly estimated by such a low-grade IMU nor can measurement values be directly obtained from the GPS receiver. In order to enhance the attitude observability, the effect originating from the difference in the locations where the IMU and the GPS antenna are fixed, which is called "lever arm effect", is utilized. The advantage of this proposed method is shown experimentally. In the experiment a comparison was made between a prototype of the proposed system, which consists of MEMS inertial sensors and a civil-use GPS receiver, and GAIA, an ultra-precise INS/GPS instrument developed by Japan Aerospace Exploration Agency (JAXA) using an experimental aircraft, MuPAL-α. The result shows that the proposed method improves the attitude accuracy, and especially the heading. Moreover, analyses of covariance matrices are performed to further investigate the effectiveness of the proposed method.

1 Introduction

The trend for navigation instruments which output the basic state values such as position, velocity, and attitude, is to become smaller, lighter and more cost-effective. This corresponds to today's demands, for example, to transfer aerospace navigation technology to consumer products such as car navigation and to guide unconventional vehicles such as small UAVs (Unmanned Aerial Vehicles) [1]. Since there is a trade-off between accuracy and other specifications – mainly size, weight, and cost – smart solutions are needed to maintain accuracy under those limitations.

Against this background, a prototype navigation system was built, which is small, light and inexpensive enough to use for controlling small UAVs in the previous work [2]. It consisted of ultra low accuracy MEMS inertial sensors and a civil-use GPS receiver. The applied algorithm, which utilized quaternions to represent terrestrial position and relative attitude, estimated the error covariance precisely even when the state was close to the singular points.

The accuracy of the prototype system was obtained by comparison with GAIA [3], which is a reliable navigation device and has about 1 meter absolute accuracy in position. Table 1 shows a summary of the result. The accuracy in position and velocity is enough for controlling a small

UAV. However, the accuracy in attitude, especially heading, is not good enough for controlling small UAVs more precisely. In addition, the estimation of drift bias of inertial sensors which was introduced after the previous work did not improve the accuracy in heading sufficiently.

Table 1. Accuracy of Previous Study

	Mean	Standard deviation	Worst
Horizontal [m]	6.44	2.97	17.0
Altitude [m]	0.85	2.10	6.90
North speed [m/s]	0.00	0.12	1.25
East speed [m/s]	0.00	0.12	−1.13
Down speed [m/s]	−0.08	0.10	−0.67
Roll [deg]	0.00	0.26	−1.19
Pitch [deg]	−0.67	1.21	−3.90
Heading [deg]	4.17	9.68	23.9

Therefore, in order to improve the accuracy of the attitude, an augmentation method which originates from the difference in the locations where the IMU and the GPS antenna are fixed is proposed, and its performance is evaluated in an experiment. In this paper, firstly, the previous algorithm for integrating INS and GPS is summarized and the new augmentation method is explained. Then, a new prototype system for the experiment is described and the experimental results are shown. Furthermore, an analysis of covariance matrices of Kalman filtering which is a fundamental algorithm of the prototype system is performed. Finally, all findings are summarized and ways to further improve the attitude accuracy are discussed.

2 Previous INS/GPS Algorithm

In this section, the previous algorithm of the INS/GPS integration is described. The algorithm uses a loosely-coupled configuration, which utilizes most processed information of the GPS receiver, i.e., position and velocity. It is based on extended Kalman filtering (EKF), and it is described by the two steps of EKF, time update and measurement update, which are elaborated in the following subsections. In the following, $\underline{x}$, $\vec{x}$ and $\tilde{q}$ represent a general column vector, a general three-dimensional vector, and a general quaternion, respectively.

2.1 Time Update

The time update is performed as time passes, and the estimated state values $\hat{\underline{x}}$ are updated with

$$\hat{\underline{x}}_{t+1} = \hat{\underline{x}}_t + \int_{\Delta t} f(\hat{\underline{x}}, \hat{\underline{u}}) \, , \tag{1}$$

where $\hat{\underline{u}}$ are the observed inputs, because the relation between the true state values $\underline{x}$ and the true inputs $\underline{u}$ is

$$\frac{d}{dt}\underline{x} \equiv f(\underline{x}, \underline{u}) \, . \tag{2}$$

In the INS/GPS algorithm, $\underline{x}$ contains 16 state variables: the velocity $\dot{\vec{r}}_e^n$, terrestrial position (i.e., latitude, longitude, and azimuth angle) $\tilde{q}_e^n$, altitude h, attitude $\tilde{q}_n^b$, and sensor biases $\underline{b}$. $\underline{u}$ contains 15 state variables and corresponds to acceleration $\vec{a}^b$, angular speed $\vec{\omega}_{b/i}^b$, gravity $\vec{g}^n$, and bias drifts $\delta\vec{b}$. That is

$$\underline{x} \equiv \begin{bmatrix} \dot{\vec{r}}_e^n \\ \tilde{q}_e^n \\ h \\ \tilde{q}_n^b \\ \underline{b} \end{bmatrix} , \quad \underline{u} \equiv \begin{bmatrix} \vec{a}^b \\ \vec{\omega}_{b/i}^b \\ \vec{g}^n \\ \delta\vec{b} \end{bmatrix} . \tag{3}$$

$\hat{\vec{a}}^b$ and $\hat{\vec{\omega}}_{b/i}^b$ are obtained from inertial sensors, that is, 3-axes accelerometers and 3-axes gyros respectively. Sensor biases $\underline{b}$ are 6 values because they are derived from the accelerometers and the gyros. They are modeled depending on the first-order Gauss Markov process:

$$\frac{d}{dt}\underline{b} = -B\underline{b} + \underline{w} , \tag{4}$$

where B is a diagonal matrix and $\underline{w}$ is white noise.

Simultaneously, the system covariance update is performed according to

$$P_{t+1} = \Phi P_t \Phi^{\mathrm{T}} + \Gamma_t Q_t \Gamma_t^{\mathrm{T}} , \tag{5}$$

where P and Q are the system error covariance and the input error covariance of the EKF respectively, i.e,

$$P \equiv E\left[\Delta\underline{x}(\Delta\underline{x})^{\mathrm{T}}\right], \quad Q \equiv E\left[\Delta\underline{u}(\Delta\underline{u})^{\mathrm{T}}\right]. \quad (6)$$

The symbol Δ represents the difference value between the estimated value and the true value, and matrices Φ, Γ are derived from Eq. (2). Here, Δx contains 14 state variables, because $\Delta\tilde{q}$ is defined with a small vector element $\Delta\vec{u}$ in the multiplicative form as in the previous study,

$$\Delta\tilde{q} \equiv \begin{Bmatrix} 1 \\ \Delta\vec{u} \end{Bmatrix} \tilde{q} - \tilde{q} \quad (7)$$

in order to keep unity of a quaternion. Therefore, $\Delta\underline{x}$ is

$$\Delta\underline{x} \equiv \Delta \begin{bmatrix} \dot{\vec{r}}_e^n \\ \vec{u}_e^n \\ h \\ \vec{u}_n^b \\ \underline{b} \end{bmatrix}, \quad (8)$$

and the system covariance matrix P is 14 by 14.

2.2 Measurement Update

The measurement update is performed when the GPS receiver outputs its observed values $\underline{z}$,

$$\underline{z} \equiv \begin{bmatrix} \dot{\vec{r}}_e^n \\ \tilde{q}_e^n \\ h \end{bmatrix}_{\mathrm{GPS}}. \quad (9)$$

The relation between $\underline{x}$ and $\underline{z}$ is called the observation equation:

$$\underline{z} = h(\underline{x}) + \underline{v}, \quad (10)$$

and it is deformed using the notation Δ:

$$\underline{z} - h(\hat{\underline{x}}) = -H_\Delta \Delta\underline{x} + \underline{v}, \quad (11)$$

where H_Δ is defined according to

$$H_\Delta \Delta\underline{x} \equiv h(\hat{\underline{x}}) - h(\underline{x}), \quad (12)$$

and $\underline{v}$ is the error of the observed value $\underline{z}$. Then, $\hat{\underline{x}}$ and P are renewed by the following equations:

$$K_t \equiv P_t H_{\Delta t}^{\mathrm{T}} (H_{\Delta t} P_t H_{\Delta t}^{\mathrm{T}} + R_t)^{-1} \quad (13)$$

$$P_t \leftarrow (I - K_t H_{\Delta t}) P_t \quad (14)$$

$$\Delta\hat{x}_t \equiv K_t (z_t - H_{\Delta t}\hat{\underline{x}}) \quad (15)$$

$$\hat{\underline{x}}_t \leftarrow \hat{\underline{x}}_t - \Delta\hat{x}_t, \quad (16)$$

where R is the observation error covariance, i.e.,

$$R \equiv E\left[\underline{v}(\underline{v})^{\mathrm{T}}\right]. \quad (17)$$

3 Augmentation Method

In this section, the reasons why the attitude could not be estimated accurately in the previous study is discussed and the augmentation method is explained.

3.1 Reasons for Low Attitude Accuracy

The degraded attitude accuracy mainly results from the low accuracy of the MEMS gyros. It is noticed that the accuracy of heading is much worse than roll and pitch. This is because roll and pitch can be corrected easily using the direction of the gravity vector which is large enough to be sensed even with such low-accuracy accelerometers. However absolute heading cannot be augmented by the gravitation, but only by the Earth's rotation rate, which is very small and can be measured only with high-grade gyros, for example, ring laser gyros (RLG) or fiber optic gyros (FOG). Thus, the precision of heading is most reflected in the gyro 's performance, and it is concluded that the poor performance of the MEMS gyros deteriorates the heading accuracy in particular.

Furthermore, the low observability of the attitude is another reason for the degraded attitude accuracy. In the previous work, the difference between the locations of the IMU and the antenna of the GPS receiver was not considered. In other words, an INS and a GPS were located at nearly the same position, and the observation equation (10) was

$$\begin{bmatrix} \dot{\vec{r}}_e^n \\ \tilde{q}_e^n \\ h \end{bmatrix}_{\mathrm{GPS}} = \begin{bmatrix} I & 0 & 0 & 0 & 0 \\ 0 & I & 0 & 0 & 0 \\ 0 & 0 & I & 0 & 0 \end{bmatrix} \begin{bmatrix} \dot{\vec{r}}_e^n \\ \tilde{q}_e^n \\ h \\ \tilde{q}_n^b \\ \underline{b} \end{bmatrix} + \underline{v}. \quad (18)$$

This equation shows that there is no hint related to attitude, because the elements in the forth column of the matrix on the right hand-side are ze-

ros. This drawback is also especially influencing the accuracy of the heading, because there is no other support for heading, unlike for roll and pitch, which can be compensated using the gravity vector.

3.2 Lever Arm Effect

Based on the discussion in the previous subsection, to improve the attitude accuracy without changing the gyros, augmentation of the observability of the attitude should be effective. Suppose that the GPS antenna is fixed at a location different from the INS. In that case, the velocity $\dot{\vec{r}}_e^n$ and position $\tilde{q}_e^n, h$ obtained by the GPS receiver are also functions of the attitude $\tilde{q}_n^b$, the offset of the antenna $\vec{l}$ (lever arm), and angular speed $\vec{\omega}_{b/n}$ (see Fig. 1). The observation equation (10) then becomes

$$\begin{bmatrix} \dot{\vec{r}}_e^n \\ \tilde{q}_e^n \\ h \end{bmatrix}_{\mathrm{GPS}} = \begin{bmatrix} I & 0 & 0 & \not{0} & \not{0} \\ 0 & I & 0 & \not{0} & 0 \\ 0 & 0 & I & \not{0} & 0 \end{bmatrix} \begin{bmatrix} \dot{\vec{r}}_e^n \\ \tilde{q}_e^n \\ h \\ \tilde{q}_n^b \\ \underline{b} \end{bmatrix} + \underline{\nu}. \quad (19)$$

where $\not{0}$ indicates a non-zero value. This equation shows that the outputs of a GPS receiver include clues of the attitude, and the coupling between attitude and other state values are tightened. The author calls this phenomenon “lever arm effect”.

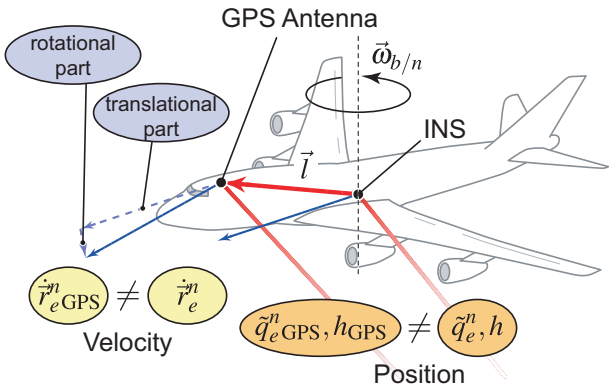

Fig. 1. Due to the "Lever Arm Effect", the output of the GPS receiver is not equal to that of INS.

Finally, Fig. 2 summarizes the algorithm of the previous study and this augmenting method. As shown in the figure, the augmentation method is performed in the measurement update.

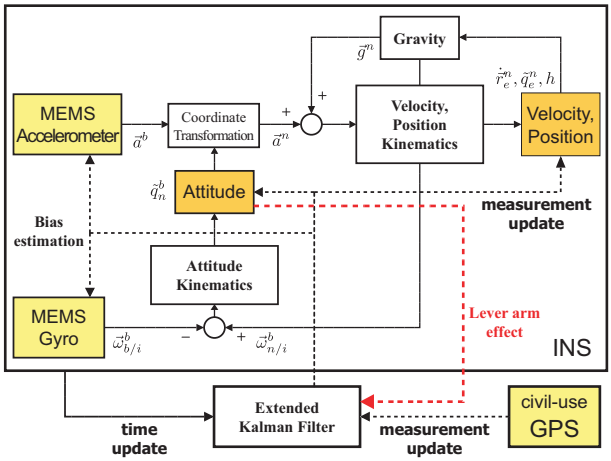

Fig. 2. INS/GPS Algorithm

4 Experiment

To show the effectiveness of the proposed method, a prototype INS/GPS system was made, and experiments were performed. In this section, the prototype system for the experiment is described firstly. Then, the experimental environment is detailed. Finally, the result is shown.

4.1 Prototype

The prototype mainly consists of MEMS inertial sensors, which has 6 degree of freedom (DOF), a L1-frequency GPS receiver, and a DSP processor. Figures 3, 4, and Table 2 show a photograph, the functional diagram, and the main components of the prototype respectively. The size of the prototype are about $50 \times 50 \times 50$mm its weight is less than 100g, which is small and light enough for installation into small UAVs. The prototype has not only the function of ING/GPS navigation, but also that of an autopilot system for small UAVs. It is functionally divided into four parts: sensor, recorder, calculation, and interface, which will be discussed consecutively.

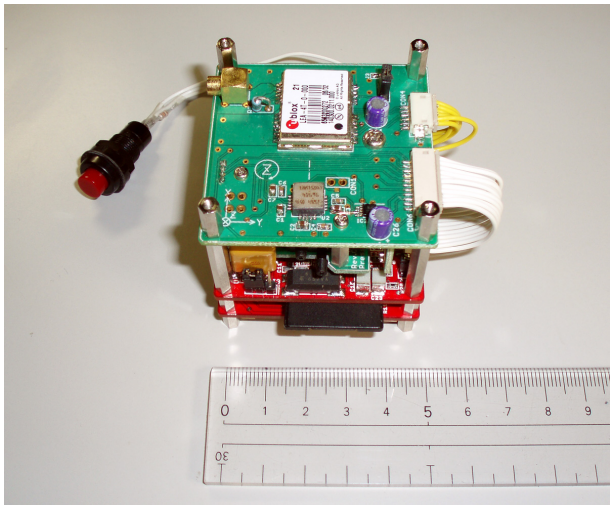

Fig. 3. Prototype (without interface part)

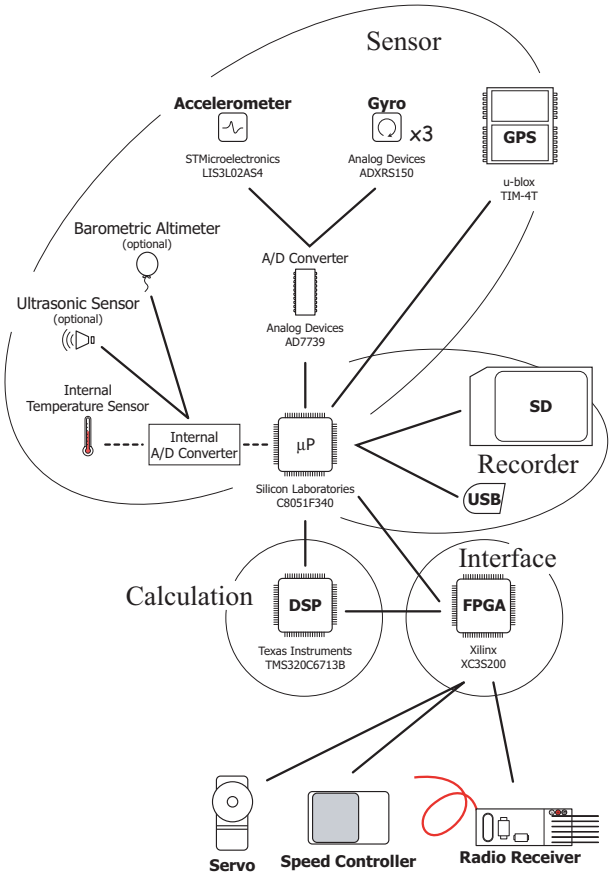

Fig. 4. Functional Diagram of Prototype

4.1.1 Sensor part

This part includes all sensors whose outputs are inputs of the INS/GPS algorithm. The tri-axes angular speed and tri-axes acceleration outputs which are measured by MEMS inertial sensors, i.e., MEMS gyros, and a MEMS accelerometer respectively, are converted into digital values by a 24-bit Analog / Digital converter (ADC) at 100 Hz. A GPS receiver solves the current position and velocity by the tracking C/A-code at 4 Hz. A temperature sensor located in the sub-processor is used for thermal correction of the inertial sensors. A barometric sensor for measuring relative altitude, and a gauge sensor for measuring relative speed against air are also available, but not used in this study.

Table 2. Main Components of Prototype

Item	Description
Accelerometer	STMicroelectronics LIS3L02AS4 (3 axes / package, MEMS)
Gyro	Analog Devices ADXRS150 (1 axis / package * 3, MEMS)
GPS receiver	u-blox TIM-4T (L1-frequency, 4 Hz output)
Processor 1 (Main)	Texas Instruments TMS320C6713B (200 MHz Floating-Point DSP)
Processor 2 (Sub)	Silicon Laboratories C8051F340 (48 MHz 8-bit Micro computer)
Glue logic	Xilinx XC3S200 (FPGA, 2M gates)

4.1.2 Recorder part

This part logs all data, for example, the raw sensors outputs and the state values which are processed by the INS/GPS algorithm. A SD card hosted by the sub processor is used to store these data, and has a capacity to log for several hours. A USB interface provides connectivity to a PC and supports to read the data stored in the SD card.

4.1.3 Calculation part

This part performs computational operations of the INS/GPS navigation with the main processor, a floating-point DSP. When the prototype system

serves as an autopilot system for small UAVs, it also provides the functionality of performing the guidance, and the control. The calculation performance of the DSP is 1600 MIPS / 1200 MFLOPS, which is powerful enough for performing the INS/GPS algorithm at several tens hertz.

4.1.4 Interface part

This part manages the connection between the prototype and external devices, such as a wireless communication unit, and servos which actuate control surfaces of small UAVs. This function is provided by a flexible programming gate array (FPGA), which reconfigures the internal circuit by software corresponding to the connected devices.

4.2 Experimental Environment

In the experiments, two units of the prototype system are used, because two GPS antennas are used for the experiment. The experiments are performed in a flight of the experimental aircraft MuPAL-α into which the prototype units and GAIA, an ultra-precise INS/GPS instrument, are installed. All inertial sensors of the prototype system are calibrated with the temperature and misalignment compensation. Figure 5 shows the locations where the prototype units, the GPS antennas which are connected to the prototype systems, and GAIA are fixed. This configuration is the same as in the previous study, except for the positioning of the GPS antennas.

After the about two-hour flight, the data gathered by the prototypes is post-processed with the proposed INS/GPS algorithm on a PC. This is for ease, even though the prototype system has computational power enough to process them in real time. In order to clarify the effectiveness of the proposed method, three cases are performed as shown in Fig. 6. The case (A) is the same as the previous study, that is, Eq. (18) is used in the measurement update. Both the case (B) and (C) are performed with the proposed method, i.e., using Eq. (19). However they use one and two antennas respectively, and the measurement update of the case (C) is performed with applying Eq. (19) twice; once to the data derived from each antenna. Every case is compared to the output of GAIA with the consideration of the difference of their fixed positions to obtain the statistical performance.

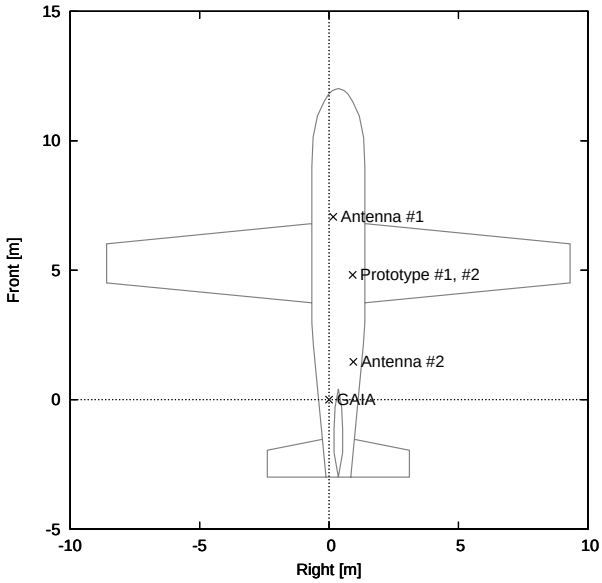

Fig. 5. Fixed Location

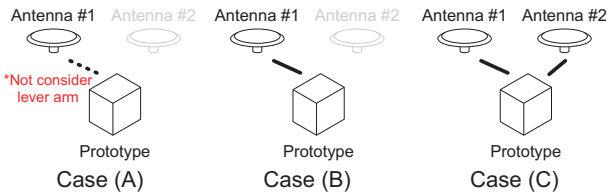

Fig. 6. Experimental Cases

4.3 Result

In any cases, the outputs of the prototype system are not diverged and are nearly equal to ones of GAIA. Figures 7–10 show a comparison of the time history of the horizontal, vertical position, the velocity, and the attitude between the case (C) of the prototype and GAIA, respectively. It is noted that the offsets in attitude result from different tilt of the surfaces where the prototype and GAIA are fixed, and they are not corrected

in the following quantitative results because the true values of them could not be measured.

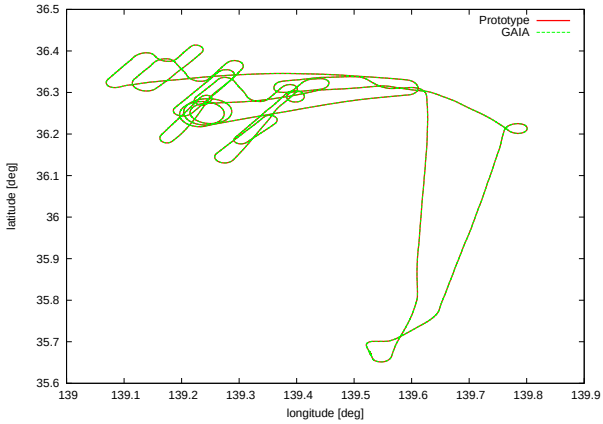

Fig. 7. Horizontal Position History

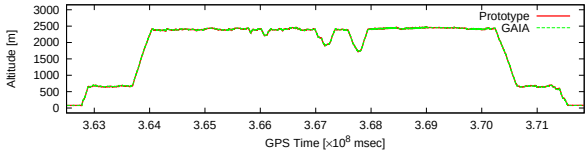

Fig. 8. Vertical Position History

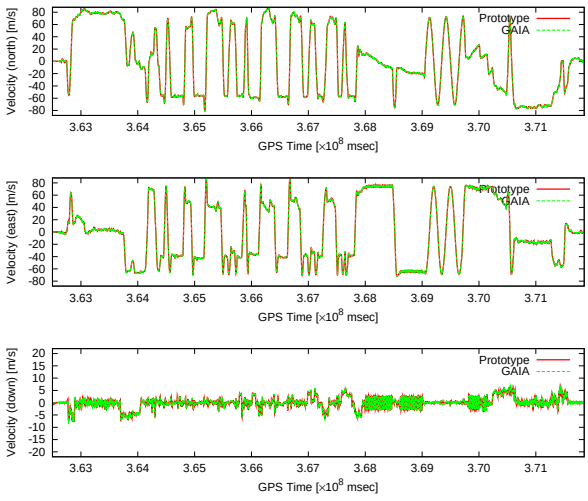

Fig. 9. Velocity History

Tables 3–5 show statistical summaries of the result. The attitude accuracy, especially in heading, is improved by using the proposed method,

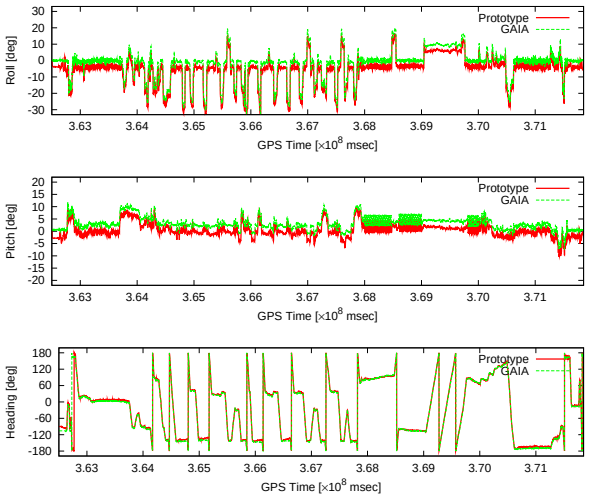

Fig. 10. Attitude History

because the standard deviations of the attitude in case (B) and (C) are smaller than in case (A).

Table 3. Case (A) Statistical Performance

	Mean	Standard deviation	Worst
Horizontal [m]	3.51	1.37	10.1
Altitude [m]	−2.97	3.05	−12.9
North speed [m/s]	−0.01	0.21	−2.90
East speed [m/s]	0.01	0.25	2.67
Down speed [m/s]	−0.03	0.22	1.70
Rolling [deg]	−3.51	0.64	−10.9
Pitching [deg]	−2.73	0.68	−5.80
Heading [deg]	0.37	4.60	31.8

In case (C), two GPS antennas are used and using the baseline made by them seems to solve the heading independently. However, this is not right, because the baseline has only 5 DOF and cannot determine the state values of a rigid body, which requires 6 DOF, that is, 3 DOF for the position and 3 DOF for the attitude. In other words, three antennas are required to solve the attitude, which is called a GPS compass. Moreover, the outputs of the GPS receiver is not accurate enough to intend for the attitude determination. Figures 11 and 12 show the histories of the relative horizontal position which are calculated

Table 4. Case (B) Statistical Performance

	Mean	Standard deviation	Worst
Horizontal [m]	2.39	1.93	12.1
Altitude [m]	−1.55	3.03	−11.5
North speed [m/s]	−0.01	0.24	−2.80
East speed [m/s]	0.01	0.27	2.99
Down speed [m/s]	−0.03	0.21	1.73
Rolling [deg]	−3.50	0.65	−11.1
Pitching [deg]	−2.83	0.53	−5.85
Heading [deg]	0.72	3.72	31.2

Table 5. Case (C) Statistical Performance

	Mean	Standard deviation	Worst
Horizontal [m]	2.41	1.83	12.2
Altitude [m]	−1.70	3.05	10.8
North speed [m/s]	−0.01	0.18	−2.13
East speed [m/s]	0.01	0.21	−2.13
Down speed [m/s]	−0.02	0.16	1.29
Rolling [deg]	−3.53	0.54	−9.49
Pitching [deg]	−2.66	0.52	−5.34
Heading [deg]	2.94	2.99	25.1

from the outputs of the prototype's GPS receivers connected to the antenna #1 and #2, respectively. The major axis of the standard deviation (1-σ) ellipsoid of them is 3.6 m. This value is a far larger error than 5mm of the carrier-phase measurement, which is used for the attitude determination in Chapter 19. of a reference book [4] and is not available for the low-cost system.

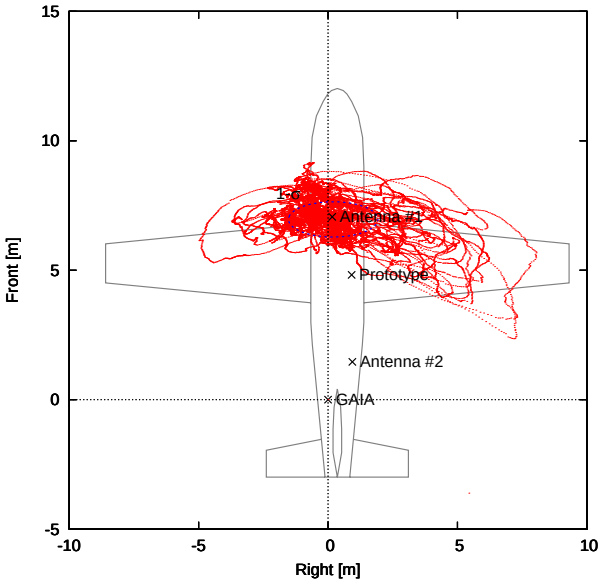

Fig. 11. GPS Position Solution (Antenna #1)

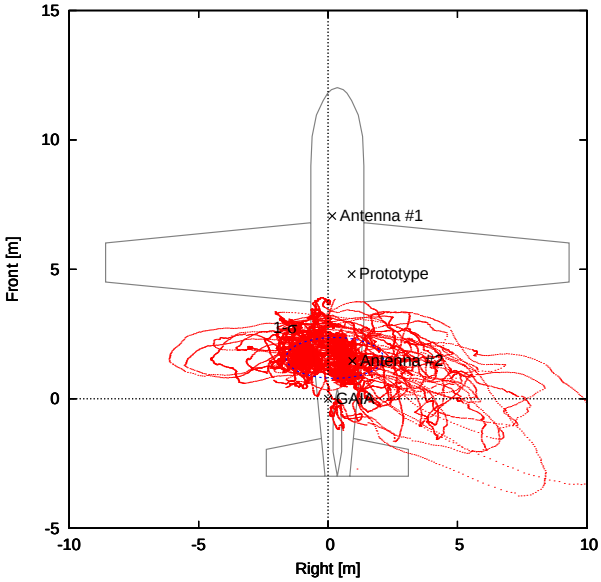

Fig. 12. GPS Position Solution (Antenna #2)

4.4 Covariance Analysis

The system error covariance matrix P defined in Eq. (6) represents how much an error seems to be included in the estimated state values when Kalman filtering performs the optimal estimation. Therefore, if the proposed method is effective, the matrix should be different for each case. Figure 13 shows the histories of some diagonal elements defined with mathematically as

$$diag\left[P_{\Delta\vec{u}_n^b}\right] \equiv diagE\left[\Delta\vec{u}_n^b\left(\Delta\vec{u}_n^b\right)^{\mathrm{T}}\right], \qquad (20)$$

which are correlated to the attitude accuracy. In case (C), these values are the smallest of all cases, which supports the fact that the statistical summaries of the attitude accuracy of case (C) are

the best results. However, there is little difference between cases (A) and (B).

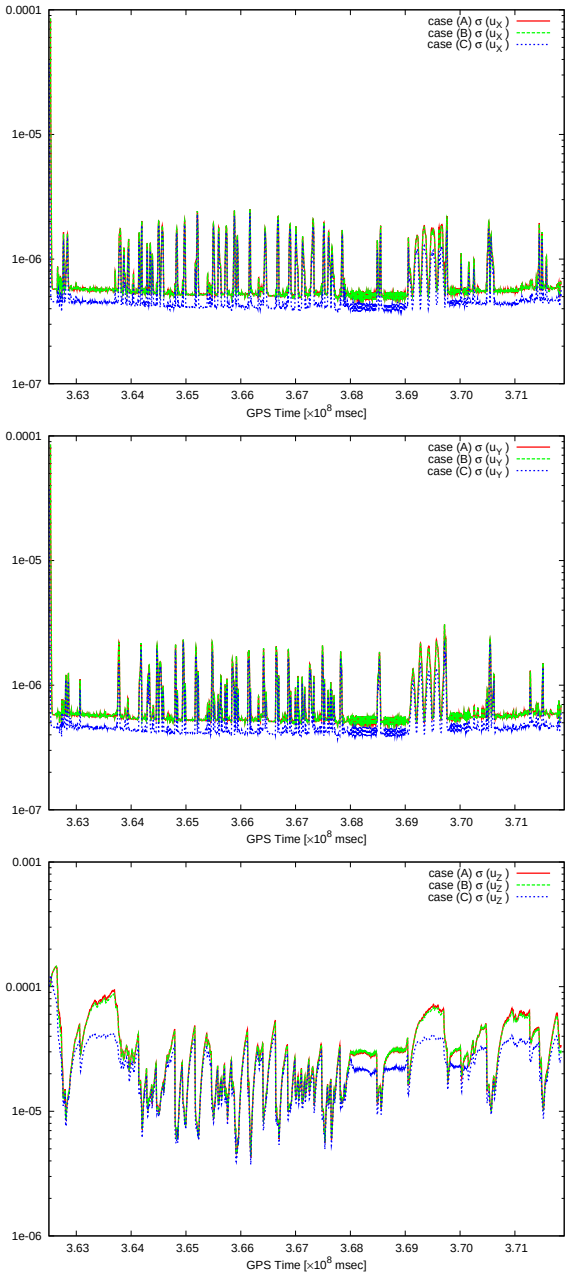

Fig. 13. Attitude Error Variance

Furthermore, a principal component analysis of the system error covariance P is conducted. This analysis decomposes P into the eigen value matrix Λ and the eigen vector matrix X as

$$P = X\Lambda X^{-1}, \tag{21}$$

where

$$X \equiv \begin{bmatrix} \underline{x}_1 & \cdots & \underline{x}_n \end{bmatrix}, \Lambda \equiv \begin{bmatrix} \lambda_1 & & 0 \\ & \ddots & \\ 0 & & \lambda_n \end{bmatrix}. \tag{22}$$

Here, the elements of the eigen vector whose principal component corresponds to the attitude error $\Delta\vec{u}_n^b$ show how much of the attitude error originates from other error sources, that is, the position and velocity error. If the realtion with other error sources is larger, there are more possibility to correct the attitude error by correcting the position and velocity error. Figure 14 shows the dependency of the attitude error in angles, where the values 0° and 45° mean no and strongest relation to other error sources respectively. This result also supports the fact that case (C) is most effective. The difference between cases (A) and (B) is also small.

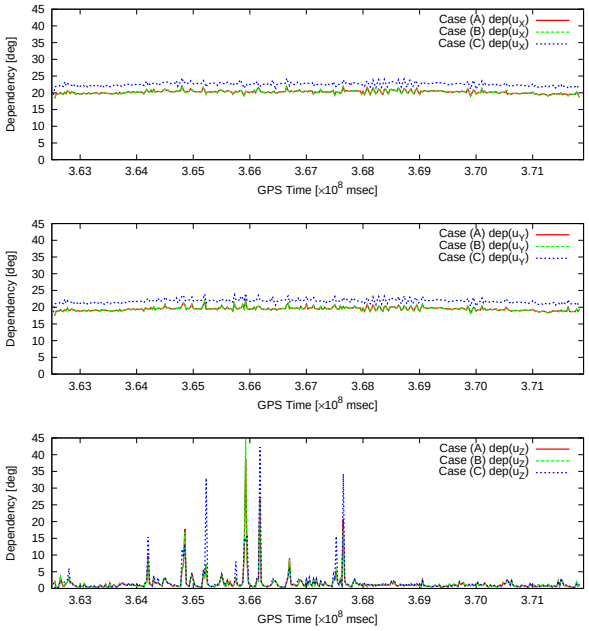

Fig. 14. Attitude Error Dependency

5 Discussion

It is concluded that the proposed method is effective, because the attitude accuracy, especially in the heading, is improved in the experiments.

In addition, it is worth to stress that even though the outputs of the GPS receiver are not accurate enough for the attitude determination, the standard deviation of the attitude error is settled to only 3° by using the proposed method with two GPS antennas.

The covariance analysis supports the fact the two GPS antennas with the proposed method is most effective. However, it cannot explain the effectiveness of the method with one GPS antenna clearly. It is thought that using one GPS antenna might decrease the error covariance of the attitude and to increase the dependency of the attitude error on other error sources, compared to the result without the proposed method. This would be due to the poor accuracy of the MEMS gyros, because the fundamental equation of the proposed method is Eq. (19), and it implicitly includes angular speed $\vec{\omega}_{b/n}$ sensed by the MEMS gyros. On the other hand, in the two antenna version, that disadvantage is recovered by their 5 DOF, which is larger than the 3 of the one antenna version, and a good result is gained in the covariance analysis.

To overcome the problem without changing the MEMS gyros, one approach is to use a longer lever arm. The longer the arm is, the larger the difference of the outputs of the GPS receiver and INS is and the easier it is to suppress the error derived from the gyros. Using more gyros also should be effective. It is possible to compose more accurate tri-axes gyro with more than three gyros by averaging because of law of great numbers.

6 Conclusion

This study proposed a method to improve the attitude accuracy of an ultra low-grade INS by utilizing GPS antenna placement. An in-flight comparison showed that the proposed method is effective to improve the attitude accuracy, especially in the heading. When using one or two antennas, the standard deviation of the heading error is improved to 3.72° or 2.99° respectively from 4.60° without the method. The covariance analysis shows that the attitude part of the system error covariance matrix is smaller by using the method with two GPS antennas. It also reveals that the poor performance of the MEMS gyro degrade the effectiveness of the proposed method.

7 Copyright Statement

References

[1] J. Liu, R. Li, X. Niu, and L. Qiao, “MEMS-Based Inertial Integrated Navigation Technology for Micro Air Vehicles ”, *Paper 2006-6547 at AIAA Guidance, Navigation, and Control Conference and Exhibit*, 2006.

[2] Naruoka, M, and Tsuchiya, T, “High performance navigation system with integration of low precision MEMS INS and general-purpose GPS”, *Transactions of the Japan Society for Aeronautical and Space Sciences, Vol.51, No.171*, 2008.

[3] Harigae, M, Tomita, H, and Nishizawa, T, “Development of High Precision GPS Aided Inertial Navigation”, *Journal of the Japan Society for Aeronautical and Space Sciences, Vol.50, No.585, pp.416-425*, 2002. (in Japanese)

[4] Paul Zarchan, “Global Positioning System: Theory and Applications Volume II”, *AIAA Education Series*, ISBN 1-56347-107-8, 1995.